Optical Materials 37 (2014) 97–103

Contents lists available at ScienceDirect

Optical Materials

journal homepage: www.elsevier.com/locate/optmat

Linear and nonlinear optical properties of α-$K_2Hg_3Ge_2S_8$ and α-$K_2Hg_3Sn_2S_8$ compounds

A.H. Reshak [a,b], Sikander Azam [a,*]

[a] New Technologies – Research Center, University of West Bohemia, Univerzitni 8, 306 14 Pilsen, Czech Republic
[b] Center of Excellence Geopolymer and Green Technology, School of Material Engineering, University Malaysia Perlis, 01007 Kangar, Perlis, Malaysia

ARTICLE INFO

Article history:
Received 26 March 2014
Received in revised form 2 May 2014
Accepted 5 May 2014
Available online 23 May 2014

Keywords:
Linear optical properties
Nonlinear optical susceptibilities
DFT

ABSTRACT

The linear and nonlinear optical properties of α-$K_2Hg_3Ge_2S_8$ and α-$K_2Hg_3Sn_2S_8$ compounds are performed using the first-principles calculations. Particularly, we appraised the optical dielectric function and the second-harmonic generation (SHG) response. We have analyzed the linear optical properties, i.e. the real and imaginary part of the dielectric tensor, the reflectivity, refractive index, extension coefficient and energy loss function. The linear optical properties show a considerable anisotropy which is important for SHG as it is defined by the phase-matching condition. The scrutiny of the roles of diverse transitions to the SHG coefficients demonstrates that the virtual electron process is foremost. The features in the spectra of $\chi^{(2)}_{322}(\omega)$ are successfully interrelated with the character of the linear dielectric function $\varepsilon(\omega)$ in terms of single-photon and two-photon resonances. In additional, we have calculated the first hyperpolarizability, β_{ijk}, for the dominant component at the static limit for the for α-$K_2Hg_3Ge_2S_8$ and α-$K_2Hg_3Sn_2S_8$ compounds. The calculated values of $\beta_{322}(\omega)$ are 2.28×10^{-30} esu for α-$K_2Hg_3Ge_2S_8$ and 3.69×10^{-30} esu for α-$K_2Hg_3Sn_2S_8$.

1. Introduction

The second harmonic generation (SHG) is described by means of the third rank polar tensors is usually forbidden by symmetry in randomly disordered media [1]. In recent times, there is much growing interest for materials with important second and third order nonlinearities as they can found use in numerous opto-electronic applications [2].

Nonlinear optical (NLO) materials play a major role as active components in a large range of applications such as optical communications, optical storage, optical computing, harmonic light generation, optical power limiting, optical rectifying devices, displays, printers, dynamic holography, frequency mixing and optical switching [3]. The majority of the early nonlinear optical (NLO) materials were based on inorganic crystals but in the last three decades the focus has shifted toward organic compounds due to their promising potential applications in optical signal processing [4,5].

The usage of the NLO to adapt the lasers to wavelength-specific applications, has boosted the demands for the novel, effective, and damage-resistant NLO materials. The fully developed crystals exists for frequency renovation of such lasers as the neodymium:yttrium aluminum garnet (Nd:YAG); though, there still need for the higher efficiencies and improved durability for the innovative materials [6]. And particularly the need is severe in the mid-(2–5 μm) and far-(>5 μm) infrared regions wherein its applications have been verified by using optical parametric oscillation (OPO), except only some materials combine the required nonlinearity, good optical transmissivity, and high resistance to optical damage in this region [7]. The non-centro-symmetric polar characteristics and simultaneous transmission of long wavelength radiation required of such crystals point to complex chalcogenides as a potential source of NLO materials. Due to a mixture of acentric arrangements the quaternary chalcogenides are much alluring and are known as the new source for nonlinear optics. They are formed from the mixture of two distinct metal centers having different size coordination preference, and packing characteristics [8]. Liao et al. accounted the series of alkali metal, quaternary chalcogenides which are based on tetrahedral anions $[SnS4]^{4-}$ and $[GeS4]^{4-}$ become stable in polysulfide fluxes [9,10]. In many cases, phases with these anions have the tendency to be non centro-symmetric, as, for example, as, for instance, $Na_{0.5}Pb_{1.75}GeS_4$ [11], $Li_{0.5}Pb_{1.75}GeS_4$ [10], $Ba_3Cd(SnS_4)_2$ [12], $Ba_6CdAg_2(SnS_4)_4$ [11], $KLnGeS_4$ [13], $KInGeS_4$ [14], $KGaGeS_4$ [15], Eu_2GeS_4 [16] and $BaAg_2GeS_4$ [17]. Probably it is conceivable that the use of these tetrahedral anions in combination with substantial elements may boost

* Corresponding author. Tel.: +420 775928620.
E-mail address: sikander.physicst@gmail.com (S. Azam).

http://dx.doi.org/10.1016/j.optmat.2014.05.006
0925-3467/

the odds of forming acentric phases [18]. In 2003 Liao et al. [19] reported the synthesis, crystal growth, spectroscopic characterization, thermal steadiness, and preliminary NLO properties of the new compounds α- and β-$K_2Hg_3Ge_2S_8$ and α- and β-$K_2Hg_3Sn_2S_8$.

In the present work we addressed ourselves to investigate the linear and nonlinear optical properties of α-$K_2Hg_3Ge_2S_8$ and α-$K_2Hg_3Sn_2S_8$ compounds using the full potential linear augmented plane wave (FPLAPW) method.

2. Computational methodology

We make use of the crystallographic data of α-$K_2Hg_3Ge_2S_8$ and α-$K_2Hg_3Sn_2S_8$ [19]. The X-ray crystallographic data of α-$K_2Hg_3Ge_2S_8$ (α-$K_2Hg_3Sn_2S_8$) show that these compounds are crystallize in noncentrosymmetric orthorhombic space group *Aba*2 (#41), with lattice parameters, $a = 19.082(2)$ Å, $b = 9.551(1)$ Å, $c = 8.2871(8)$ Å, $\alpha = 90.00$, $\beta = 90.3250$, and $\gamma = 90.00$ ($a = 19.563(2)$ Å, $b = 9.853(1)$ Å, $c = 8.467(1)$ Å, $\alpha = 90.00$, $\beta = 90.3250$, and $\gamma = 90.00$). The unit cell of crystal structures are shown in Fig. 1. We have applied the full potential linear augmented plane wave (FPLAPW) method as embodied in WIEN2k code [20]. This is an accomplishment of the density functional theory (DFT) [21,22] with different possible approximations for the exchange–correlation (XC) potential. Exchange and correlation potential was described by the local density approximation (LDA) and generalized gradient approximation (GGA) [23,24]. In additional we have used the Engel–Vosko generalized gradient approximation (EV-GGA) [25] to avoid the well-known LDA and GGA underestimation of the band gaps. On the basis of the linear APW's the Kohn–Sham equations were resolved. Within the muffin-tin (MT) spheres the potential and charge density distributions are extended in spherical harmonics with orbital number $l_{max} = 10$. The MT sphere radii of α-$K_2Hg_3Ge_2S_8$ and α-$K_2Hg_3Sn_2S_8$ were chosen to be 2.0 a.u. for K, Hg, Ge/Sn, and S, respectively. Self-consistency is obtained using $200\vec{k}$ points in the irreducible Brillouin zone (IBZ). We have calculated the linear optical susceptibilities using $500\vec{k}$ points and the nonlinear optical properties using $1000\vec{k}$ points in the IBZ.

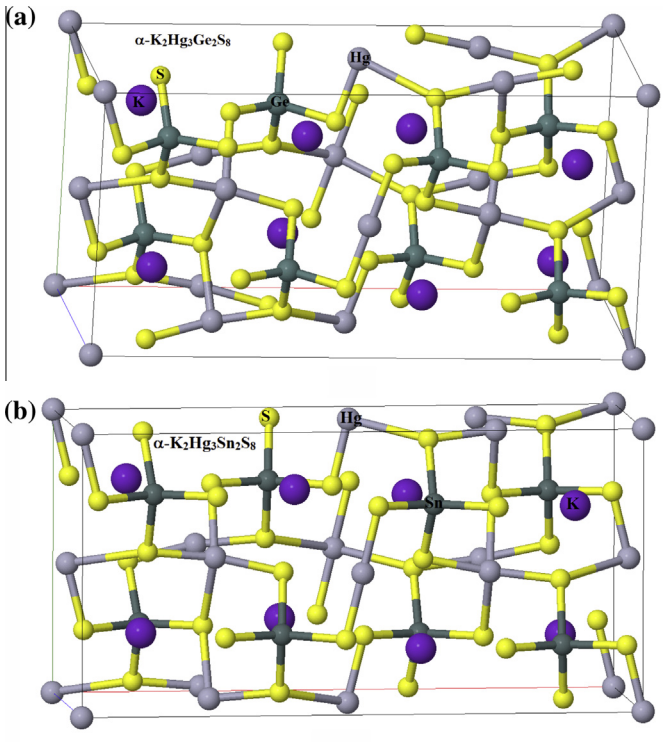

Fig. 1. Unit cell structure (a) α-$K_2Hg_3Sn_2S_8$ compound and (b) α-$K_2Hg_3Sn_2S_8$ compound. These compounds crystallize in noncentrosymmetric orthorhombic space group *Aba*2 (#41), lattice parameters of α-$K_2Hg_3Sn_2S_8$ compound are; $a = 19.082(2)$ Å, $b = 9.551(1)$ Å, $c = 8.2871(8)$ Å, $\alpha = 90.00$, $\beta = 90.3250$, and $\gamma = 90.00$. While for α-$K_2Hg_3Sn_2S_8$ compound are; $a = 19.563(2)$ Å, $b = 9.853(1)$ Å, $c = 8.467(1)$ Å, $\alpha = 90.00$, $\beta = 90.3250$, and $\gamma = 90.00$).

3. Results and discussion

3.1. Linear optical properties

The imaginary part of the dielectric function $\varepsilon_2(\omega)$ can be calculated from the momentum matrix elements between the occupied and unoccupied wave-functions, giving rise to the selection rules. The real part $\varepsilon_1(\omega)$ of the dielectric function can be assessed from the imaginary part by using the Kramers–Kronig relationship [26]. In view of the fact that EVGGA brings the calculated energy gaps (1.83 eV for α-$K_2Hg_3Ge_2S_8$ and 1.60 eV for α-$K_2Hg_3Sn_2S_8$) close to the experimental one (2.64 eV for α-$K_2Hg_3Ge_2S_8$ and 2.40 eV for α-$K_2Hg_3Sn_2S_8$) [19]. Thus, with this perspective we will focus on the EVGGA results for demonstrating the linear optical properties.

Since the investigated compounds have orthorhombic symmetry, as a result there are only three tensor components to describe whole optical properties. These are $\varepsilon_2^{xx}(\omega)$, $\varepsilon_2^{yy}(\omega)$ and $\varepsilon_2^{zz}(\omega)$ as illustrated in Fig. 2a and b. The main peaks position of $\varepsilon_2^{xx}(\omega)$, $\varepsilon_2^{yy}(\omega)$ and $\varepsilon_2^{zz}(\omega)$ spectra are given in Table 1.

Our scrutiny of the $\varepsilon_2(\omega)$ curve demonstrates that the first optical critical point of the dielectric function arises at 2.0 (1.4) eV for α-$K_2Hg_3Ge_2S_8$ (α-$K_2Hg_3Sn_2S_8$) compounds. These points are the threshold (absorption edge) for the optical transitions between the valence band maximum and the conduction band minimum. After the first critical points, the curve rises speedily. This is due to the fact that the number of points contributing toward $\varepsilon_2(\omega)$ is increased abruptly. The estimated values of the static optical dielectric constant $\varepsilon_1^{xx}(0)$, $\varepsilon_1^{yy}(0)$ and $\varepsilon_1^{zz}(0)$, which is also called higher frequency dielectric constant because it does not include the phonon effect, are listed in Table 1.

The refractive index n, is the most imperative and also significant substantial factor associated to the microscopic atomic interactions. From hypothetical perspective, there are principally two diverse looms of screening this subject: the refractive index will be related to the density and the local polarizability of these entities [27]. Alternatively, taking into consideration the crystalline structure which is symbolized by a delocalised depiction, n will be intimately connected to the energy band structure of the substances, quantum mechanical scrutiny necessities is intricate and the attained results are very fastidious. As a result, a lot of efforts have been made in order to narrate the refractive index and the energy gap E_g through simple relationships [28–33].

The refractive index $n(\omega)$ of an insulating crystal is the square root of the electric part of the dielectric constant at zero frequency, i.e. $n = \sqrt{\varepsilon_0}$, where $\varepsilon_0 = \varepsilon_1(\hbar\omega = 0)$. The intended nonzero tensor components of static refractive index $n^{xx}(0)$, $n^{yy}(0)$ and $n^{zz}(0)$ of the investigated compounds are assessed from Fig. 3(a and b) and are listed in Table 1.

The absorption coefficient $I(\omega)$ for the two compounds has been illustrated in Fig. 3(c and d). The first peaks of $I^{xx}(\omega)$, $I^{yy}(\omega)$ and $I^{zz}(\omega)$ are summarized in Table 1. For α-$K_2Hg_3Ge_2S_8$ and α-$K_2Hg_3Sn_2S_8$ compounds, the earliest absorption peaks in $I(\omega)$ spectra are originated in the range of 3.0–4.0 eV. The most imperative factor in stating the energy loss of a prompt electron peregrination in a material is the electron energy-loss function $L(\omega)$. The energy loss function $L^{xx}(\omega)$, $L^{yy}(\omega)$ and $L^{zz}(\omega)$, of the investigated compounds are demonstrated in Fig. 3(e and f). The energy loss function is plotted in basal-plane and in direction of ***c***-axis. There are other

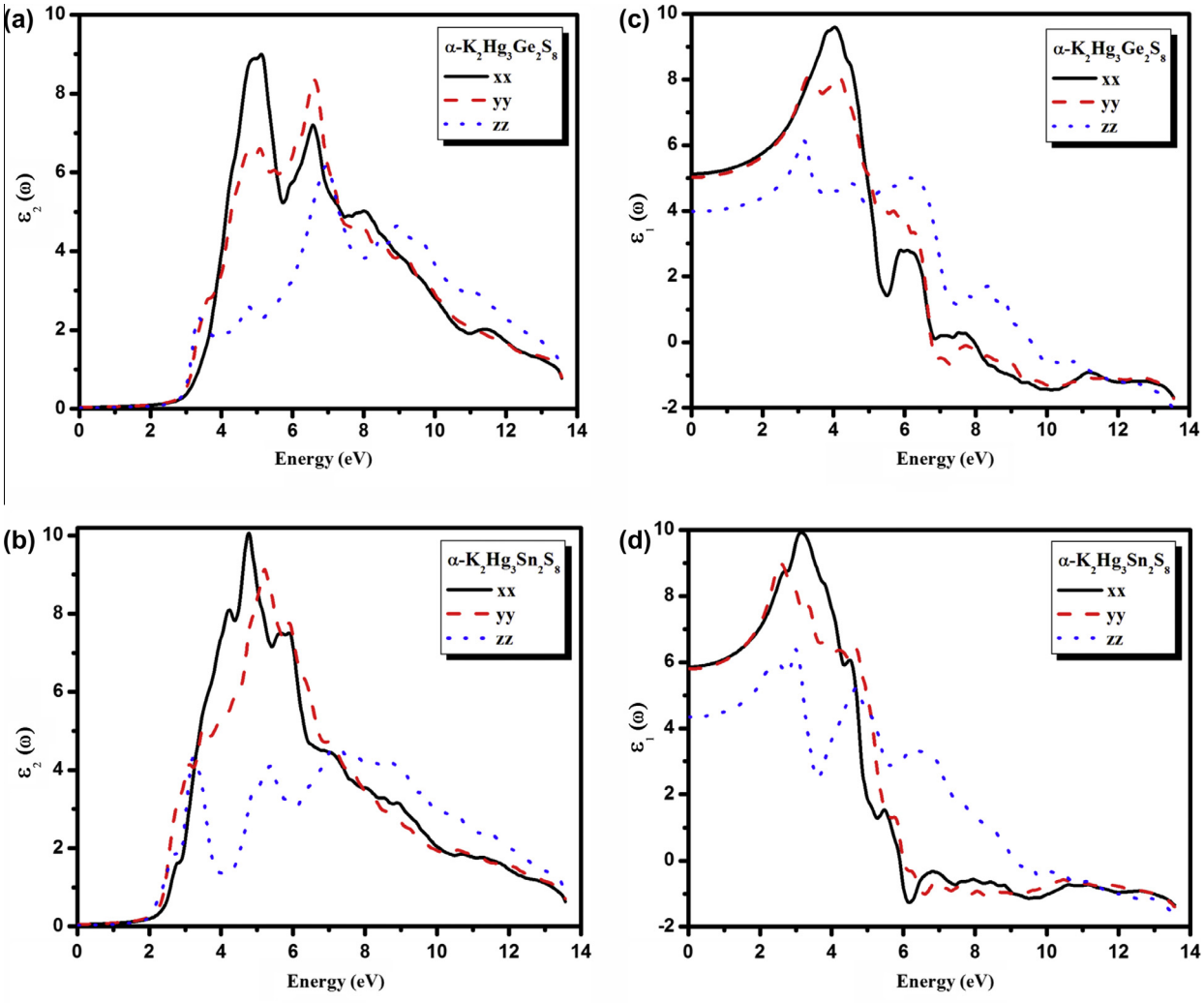

Fig. 2. Calculated imaginary $\varepsilon_2^{xx}(\omega)$, $\varepsilon_2^{yy}(\omega)$, $\varepsilon_2^{zz}(\omega)$ and real $\varepsilon_1^{xx}(\omega)$, $\varepsilon_1^{yy}(\omega)$, $\varepsilon_1^{zz}(\omega)$ parts of dielectric tensor for; (a) α-$K_2Hg_3Sn_2S_8$ compound; (b) α-$K_2Hg_3Sn_2S_8$ compound.

Table 1
Calculated dielectric constant $\varepsilon_1(0)$, refractive index $n(0)$, main peak in $\varepsilon_2(0)$, first peak in $I(\omega)$, $I(\omega)$ at the first peak for $K_2Hg_3Sn_2S_8$ and α-$K_2Hg_3Sn_2S_8$ compounds.

Compound		α-$K_2Hg_3Ge_2S_8$	α-$K_2Hg_3Sn_2S_8$
$\varepsilon_1(0)$	$\varepsilon_1^{xx}(0)$	5.12	5.85
	$\varepsilon_1^{yy}(0)$	5.01	5.79
	$\varepsilon_1^{zz}(0)$	3.97	4.33
$n(0)$	$n^{xx}(0)$	2.26	2.42
	$n^{yy}(0)$	2.23	2.41
	$n^{zz}(0)$	1.99	2.08
Position of the main peaks in $\varepsilon_2(\omega)$ in (eV)	$\varepsilon_2^{xx}(\omega)$	5.0	4.8
	$\varepsilon_2^{yy}(\omega)$	6.7	5.0
	$\varepsilon_2^{zz}(\omega)$	7.0	7.0
First peak in $I(\omega)$ in (eV)	$I^{xx}(\omega)$	13.56	13.56
	$I^{yy}(\omega)$	13.56	13.56
	$I^{zz}(\omega)$	13.56	13.56
The amplitudes of the first peak in $I(\omega)$ (10^4 cm^{-1})	$I^{xx}(\omega)$	180	177
	$I^{yy}(\omega)$	180	170
	$I^{zz}(\omega)$	180	168

features in this spectrum, in addition to the plasmon peak, associated with inter-band transitions. The plasmon peak is usually the most intense feature in the spectrum and this is at energy where $\varepsilon_1(\omega)$ goes to zero. The energy of the maximum peak of $(-\varepsilon_1(\omega))^{-1}$ is observed at ~12.5 eV for $L^{xx}(\omega)$, $L^{yy}(\omega)$ and $L^{zz}(\omega)$ which are assigned to the energy of volume plasmon $\hbar\omega_p$.

The reflectivity spectra $R(\omega)$ for both compounds, beside the three crystal components has been calculated as exposed in Fig. 3(g and h). The values of $R^{xx}(0)$, $R^{yy}(0)$ and $R^{zz}(0)$ are 0.12 (0.13), 0.14 (0.16) and 0.15 (0.17) for $K_2Hg_3Sn_2S_8$ (α-$K_2Hg_3Sn_2S_8$). The maximum peak lies in the high energy range and arises from the interband transition. These materials possess reflectivity in a wide energy (frequency) range, the disparity of reflectivity with high energy is appropriate for Bragg's reflector. We should emphasize that there exists a considerable anisotropy between three components of all optical properties along the spectral region.

3.2. Nonlinear optical properties

We also calculated the second-order nonlinear optical (NLO) susceptibilities dispersion, that is, the optical second harmonic generation (SHG). Here we will demonstrate the influence of substituting Ge by Sn atom on the nonlinear optical properties. As it is well established that the nonlinear optical properties are very sensitive to small changes in the energy band gap than the linear optical one. Since EV-GGA brings the energy gap close to the experimental one, therefore we have used a quasi-particle self-energy correction at the level of scissors operators in which the

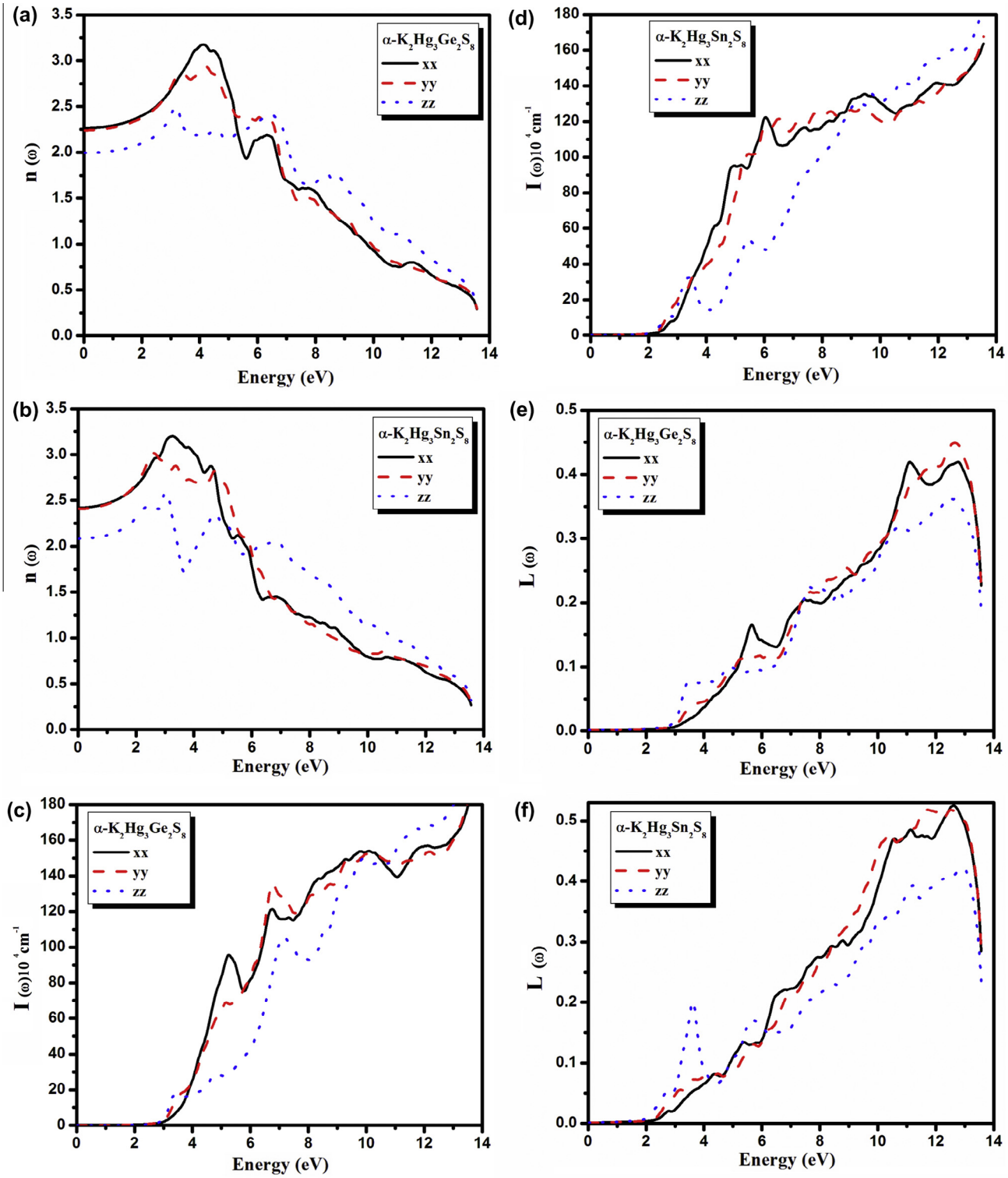

Fig. 3. Calculated energy-loss spectrum $L^{xx}(\omega)$, $L^{yy}(\omega)$, $L^{zz}(\omega)$, reflectivity $R^{xx}(\omega)$, $R^{yy}(\omega)$, $R^{zz}(\omega)$ and the refractive index $n^{xx}(\omega)$, $n^{yy}(\omega)$, $n^{zz}(\omega)$ for α-$K_2Hg_3Sn_2S_8$ and α-$K_2Hg_3Sn_2S_8$ compounds.

energy bands are rigidly shifted to merely bringing the calculated energy gap closer to the experimental value [19].

The relations for the complex second order nonlinear optical are presented in the previous studies [34,35]. Since the investigated compounds are crystallize in noncentrosymmetric orthorhombic space group, thus symmetry allows only five nonzero complex second-order NLO susceptibility tensor components. These are $\chi^{(2)}_{131}(\omega)$, $\chi^{(2)}_{232}(\omega)$, $\chi^{(2)}_{311}(\omega)$, $\chi^{(2)}_{322}(\omega)$ and $\chi^{(2)}_{333}(\omega)$. The dispersal of these components have been demonstrated in Fig. 4(a and b). These figures suggest that the $|\chi^{(2)}_{322}(\omega)|$ component is the dominant one for α-$K_2Hg_3Ge_2S_8$ and α-$K_2Hg_3Sn_2S_8$. The value of $|\chi^{(2)}_{322}(0)|$ for α-$K_2Hg_3Ge_2S_8$ and α-$K_2Hg_3Sn_2S_8$ are 6.42 and 9.69 pm/V.

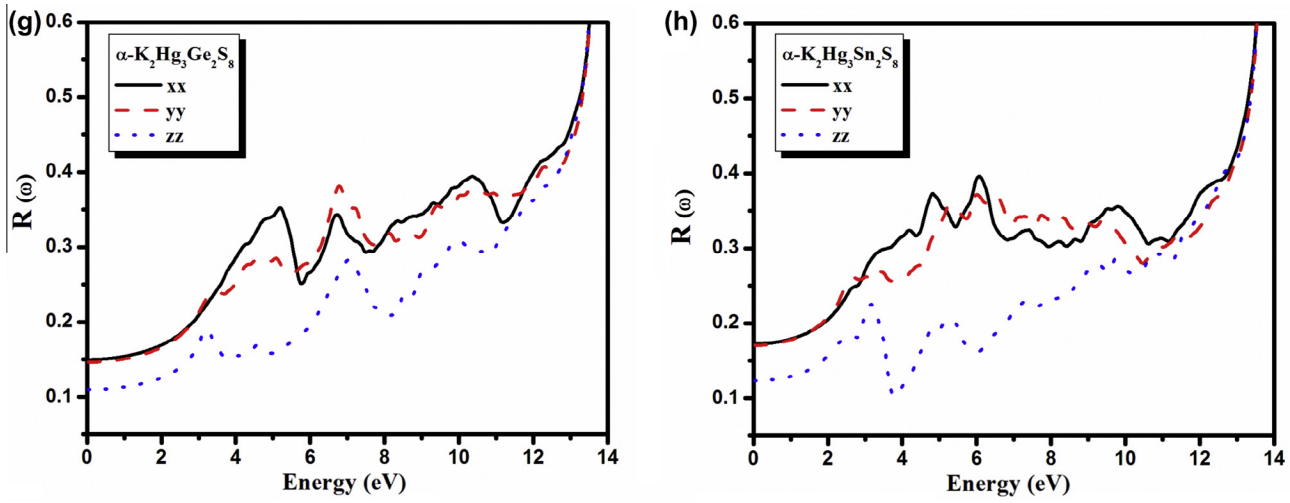

Fig. 3 (*continued*)

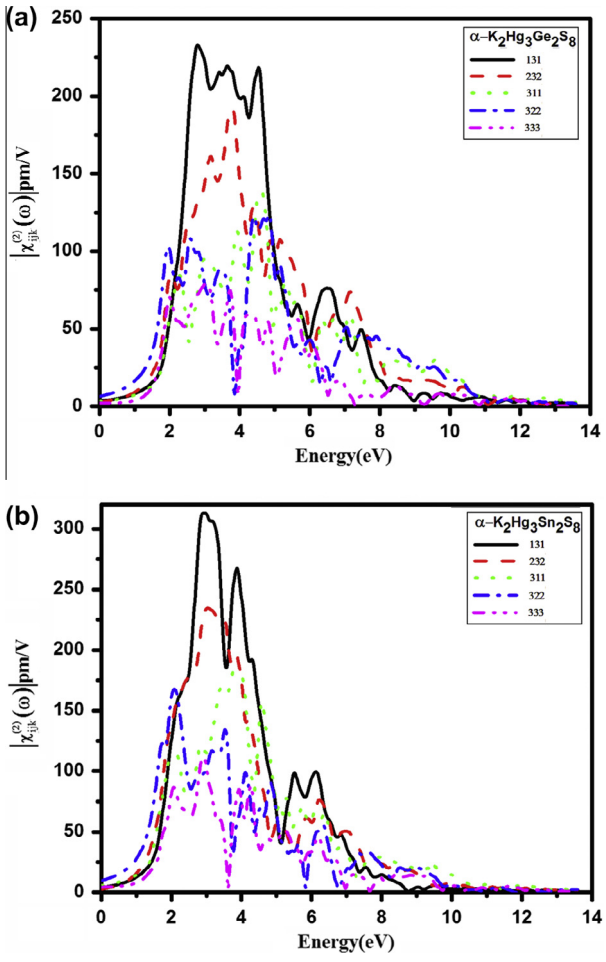

Fig. 4. Calculated $|\chi^{(2)}_{ijk}(\omega)|$ for five components namely; $|\chi^{(2)}_{131}(\omega)|$, $|\chi^{(2)}_{232}(\omega)|$, $|\chi^{(2)}_{311}(\omega)|$, $|\chi^{(2)}_{322}(\omega)|$ and $|\chi^{(2)}_{333}(\omega)|$ for (a) α-$K_2Hg_3Sn_2S_8$ and (b) α-$K_2Hg_3Sn_2S_8$ compounds.

Fig. 5a and b, illustrated the real and imaginary parts of the dominant component $\chi^{(2)}_{322}(\omega)$. It is clear that the imaginary part of the SHG is zero below half the band gap. The 2ω terms begin to contribute at energies $\sim \frac{1}{2}E_g$ and the ω terms for energy values above E_g. Fig. 5c shows the $|\chi^{(2)}_{322}(\omega)|$ of α-$K_2Hg_3Ge_2S_8$ and α-$K_2Hg_3Sn_2S_8$. Following Fig. 5a–c, we highlighted that substituting Ge by Sn cause to increase the amplitude and shift all the structures of $\chi^{(2)}_{ijk}(-2\omega;\omega;\omega)$ toward lower energies, indicated that replacing Ge by Sn led to increase the SHG value. Reference to Fig. 5c, it is cleared that the $|\chi^{(2)}_{322}(0)|$ values increases from 6.42 to 9.69 pm/V with substituting Ge by Sn.

We should emphasize that due to the presence of 2ω and ω terms it is very difficult to analyze the complex second-order nonlinear optical susceptibility tensors using the calculated electronic band structure. Therefore we will use our calculated $\varepsilon_2(\omega)$ as a function of both $\omega/2$ and ω to identify the spectral features of the dominant component $|\chi^{(2)}_{322}(\omega)|$. Fig. 6 illustrates the dominant component $|\chi^{(2)}_{322}(\omega)|$ (upper panel) along with $\varepsilon_2(\omega)$ as a function of both $\omega/2$ and ω (lower panel) for α-$K_2Hg_3Ge_2S_8$ and α-$K_2Hg_3Sn_2S_8$. The spectral structure of $|\chi^{(2)}_{322}(\omega)|$ located in the energy range 1.32 (1.2) −3.0 eV for α-$K_2Hg_3Ge_2S_8$ (α-$K_2Hg_3Sn_2S_8$) is originated from 2ω resonance. The next spectral structure of $|\chi^{(2)}_{322}(\omega)|$ between 3.0 and 7.0 eV is associated with interference between 2ω and ω resonances. The third spectral structure of $|\chi^{(2)}_{322}(\omega)|$ from 7.0 eV and above is mainly due to ω resonance. Fig. 7(a and b) interprets the 2ω inter/intra band in addition to 1ω inter/intra band support to the imaginary part of the nonlinear optical susceptibilities for both compounds. Finally, we have calculated the microscopic first hyperpolarizability, β_{ijk} for the dominant component at the static limit for the for α-$K_2Hg_3Ge_2S_8$ and α-$K_2Hg_3Sn_2S_8$ compounds. The calculated values of $\beta_{322}(\omega)$ are 2.28×10^{-30} esu for α-$K_2Hg_3Ge_2S_8$ and 3.69×10^{-30} esu for α-$K_2Hg_3Sn_2S_8$.

4. Conclusions

In short description, linear and nonlinear optical susceptibilities of α-$K_2Hg_3Sn_2S_8$ (α-$K_2Hg_3Sn_2S_8$) compounds were calculated by means of the density functional theory based on the full potential linear augmented plane wave (FPLAPW) technique. We analyzed the linear optical properties, i.e. the real and imaginary part of the dielectric tensor along with the other related properties like reflectivity, refractive index, extension coefficient and energy loss function. From the study of the reflectivity we concluded that this material can be used as shielding material at higher energies. In additional to the linear properties we also calculated the second order nonlinear optical properties namely the SHG. Where we

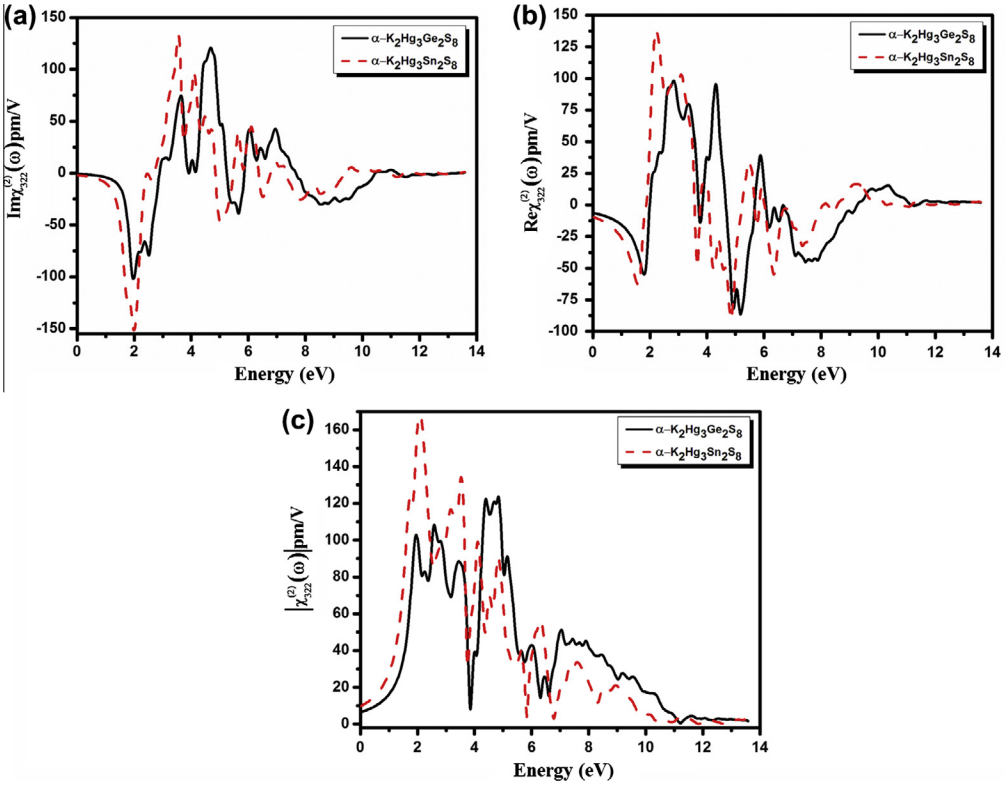

Fig. 5. (a) Calculated imaginary part of $\chi^{(2)}_{322}(\omega)$ for α-$K_2Hg_3Sn_2S_8$ and α-$K_2Hg_3Sn_2S_8$ compounds; (b) calculated real part of $\chi^{(2)}_{322}(\omega)$ for α-$K_2Hg_3Sn_2S_8$ and α-$K_2Hg_3Sn_2S_8$ compounds; (c) calculated $|\chi^{(2)}_{322}(\omega)|$ for α-$K_2Hg_3Sn_2S_8$ and α-$K_2Hg_3Sn_2S_8$ compounds.

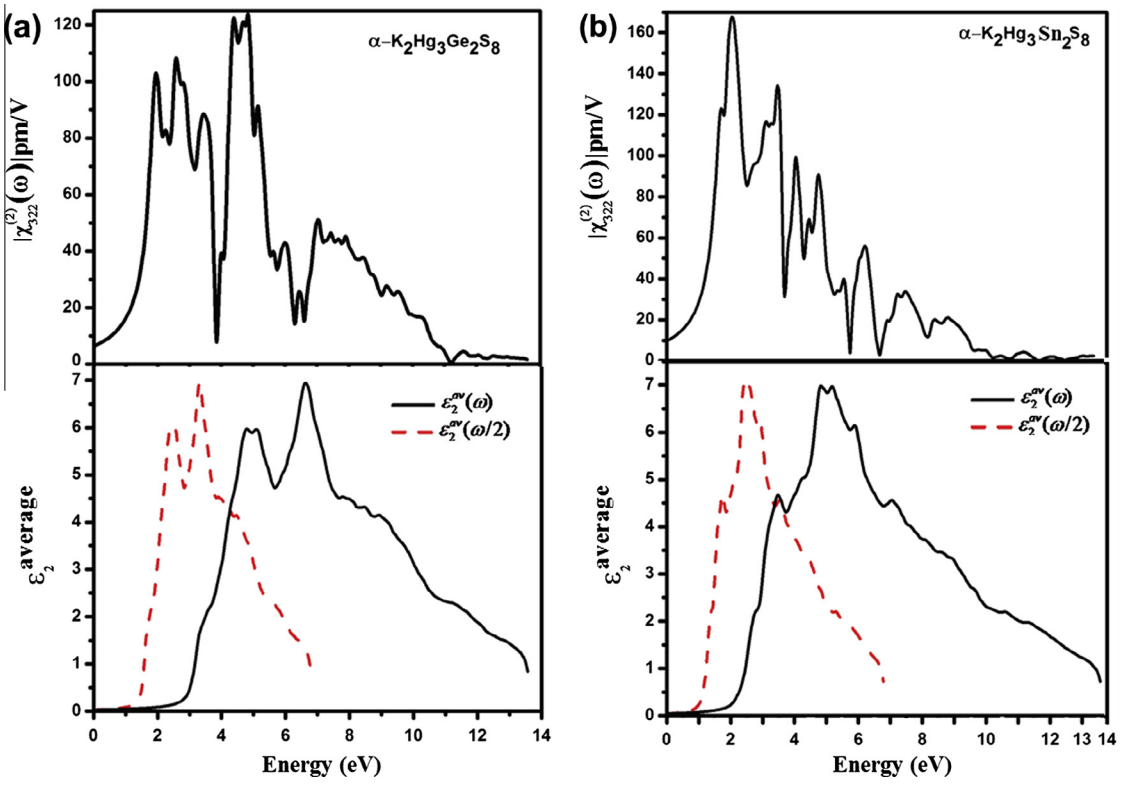

Fig. 6. Calculated $|\chi^{(2)}_{322}(\omega)|$ and $\varepsilon_2^{\text{average}}(\omega)$ along with $\varepsilon_2^{\text{average}}(\omega/2)$.

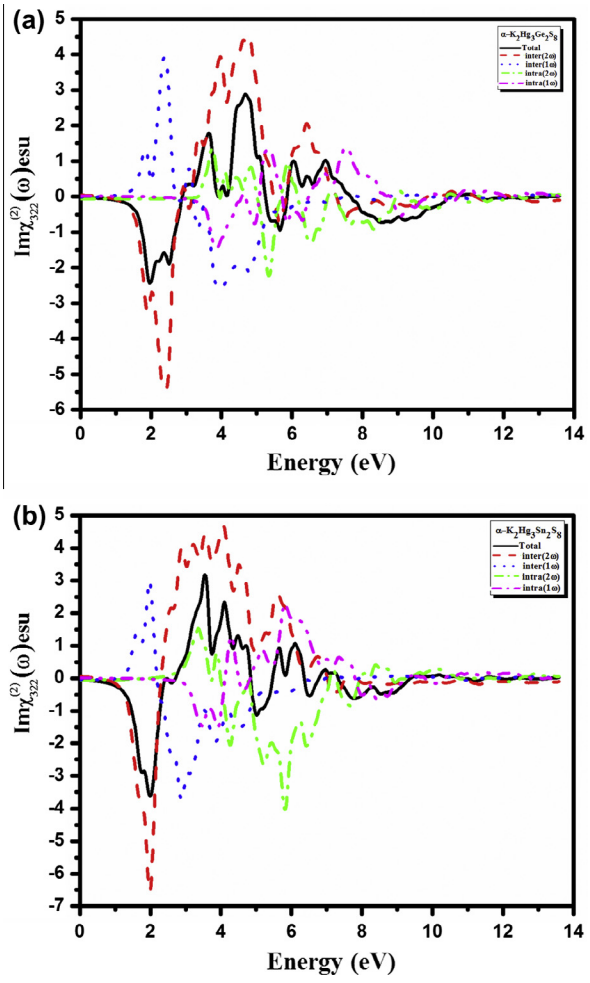

Fig. 7. Calculated imaginary part of $\chi^{(2)}_{322}(\omega)$ along with inter ($2\omega/\omega$) and intra ($2\omega/\omega$) band contribution for (a) α-$K_2Hg_3Sn_2S_8$ compound and (b) α-$K_2Hg_3Sn_2S_8$ compound.

found that $\chi^{(2)}_{322}(\omega)$ is the dominant component. From the value of $\chi^{(2)}_{322}(\omega)$ we have obtained first hyperpolarizability, β_{322} for the dominant component.

Acknowledgements

The result was developed within the CENTEM project, Reg. No. CZ.1.05/2.1.00/03.0088, co-funded by the ERDF as part of the Ministry of Education, Youth and Sports OP RDI program.

References

[1] Iliopoulos et al., Appl. Phys. Lett. 103 (2013) 231103.
[2] J. Phys, Chem. B 108 (39) (2004) 14943.
[3] I. Guezguez, A. Karakas, K. Iliopoulos, B. Derkowska-Zielinska, A. El-Ghayoury, A. Ranganathan, P. Batail, A. Migalska-Zalas, B. Sahraoui, M. Karakaya, Opt. Mater. 36 (2014) 106–111.
[4] P.S.P. Silva et al., Chem. Phys. 428 (2014) 67–74.
[5] A. Zawadzka et al., Dyes Pigm. 101 (2014) 212e220.
[6] (a) D.A. Keszler, Curr. Opin. Solid State Mater. Sci. 1 (2) (1996) 204–211;
(b) P. Becker, Adv. Mater. 10 (13) (1998) 979.
[7] (a) F. Rotermund, V. Petrov, F. Noack, Opt. Commun. 185 (2000) 177–183;
(b) B.J. Zhao, S.F. Zhu, Y.D. Li, F.L. Yu, Q.F. Li, Z.H. Li, X.H. Zhu, S.Y. Shao, Lin, J. Opt. Eng. 38 (12) (1999) 2129–2133;
(c) V.V. Apollonov, S.P. Lebedev, G.A. Komandin, Y.A. Shakir, V.V. Badikov, Y.M. Andreev, A.I. Gribenyukov, Laser Phys. 9 (1999) 1236–1239;
(d) K.L. Vodopyanov, J.P. Maffetone, I. Zwieback, W. Ruderman, Appl. Phys. Lett. 75 (1999) 1204–1206;
(e) V.A. Gorobets, V.O. Petukhov, S.Y. Tochitskii, V.V. Churakov, J. Opt. Technol. 66 (1999) 53–57.
[8] (a) M.G. Kanatzidis, J.H. Liao, Marking G A Alkali Metal Quaternary Chalcogenides and Process for the Preparation Thereof, United States Patent 5,614,128.;
(b) M.G. Kanatzidis, J.-H. Liao, Marking G A Alkali Metal Quaternary Chalcogenides and Process for the Preparation Thereof, United States Patent 5,618,471.
[9] J.-H. Liao, M.G. Kanatzidis. (Submitted for publication).
[10] (a) J.A. Aitken, P. Larson, S.D. Mahanti, M.G. Kanatzidis, Chem. Mater. 13 (2001) 4714–4721;
(b) Y. Matsushita, M.G.Z. Kanatzidis, Naturforsch. B 53b (1998) 23–30.
[11] J.A. Aitken, G.A. Marking, M. Evain, L. Iordanidis, M.G. Kanatzidis, J. Solid State Chem. 2000 (153) (2000) 158–169.
[12] C.L.Z. Teske, Anorg. Allg. Chem. 522 (1985) 122–130.
[13] (a) P. Wu, J.A. Ibers, J. Solid State Chem. 107 (1993) 347;
(b) G. Gauthier, F. Guillen, S. Jobic, P. Deniard, P. Macaudiere, C. Fouassier, R. Brec, Compt. Rend. Acad. Sci. Ser. II 2 (1999) 611.
[14] W. Klemm, H. Sodomann, P.Z. Langmesser, Anorg. Allg. Chem. 241 (1939) 281–304.
[15] B. Krebs, Angew. Chem. Int. Ed. Engl. 22 (1983) 113–134.
[16] M. Tampier, D.J. Johrendt, Solid State Chem. 158 (2) (2001) 343–348.
[17] D. Müller, H.Z. Hahn, Anorg. Allg. Chem. 438 (1978) 258.
[18] P.S. Halasyamani, K.R. Peoppelmeier, Chem. Mater. 10 (1998) 2753–2769.
[19] J.-H. Liao, G.M. Marking, K.F. Hsu, Y. Matsushita, M.D. Ewbank, R. Borwick, P. Cunningham, M.J. Rosker, M.G. Kanatzidis, J. Am. Chem. Soc. 125 (31) (2003) 9485.
[20] P. Blaha, K. Schwarz, J. Luitz, WIEN97, a Full Potential Linearized Augmented Plane Wave Package for Calculating Crystal Properties, Karlheinz Schwarz, Techn. Universit at Wien, Austria, 1991 (ISBN:3-9501031-0-4).
[21] P. Hohenberg, W. Kohn, Phys. Rev. 136 (1996) B864.
[22] W. Kohn, L.J. Shom, Phys. Rev. 140 (1965) A1133.
[23] J.P. Perdew, A. Zunger, Phys. Rev. B 23 (1981) 5048.
[24] J.P. Perdew, K. Burke, M. Ernzerhof, Phys. Rev. Lett. 77 (1996) 3865.
[25] E. Engel, S.H. Vosko, Phys. Rev. B 50 (1994) 10498.
[26] Sikander Azam, Jiri Bila, H. Kamarudin, A.H. Reshak, Int. J. Electrochem. Sci. 9 (2014) 445–459.
[27] N.M. Balzaretti, J.A.H. Da Jornada, Solid State Commun. 99 (1996) 943.
[28] T.S. Moss, Proc. Phys. Soc. B 63 (1950) 167.
[29] V.P. Gupta, N.M. Ravindra, Phys. Status Solidi B 100 (1980) 715.
[30] A.L. Ruoff, Mater. Res. Soc. Symp. Proc. 22 (1984) 287.
[31] R.R. Reddy, S. Anjaneyulu, C.L.N. Samara, J. Phys. Chem. Solid 54 (1993) 635.
[32] P. Herve, L.K.J. Vandamme, Infrared Phys. Technol. 35 (1993) 609.
[33] N.M. Ravindra, S. Auluck, V.K. Srivastava, Phys. Status Solidi B 93 (1979) K155.
[34] A.H. Reshak, W. Khan, J. Alloys Compd. 592 (2014) 92–99.
[35] A.H. Reshak, Saleem Ayaz Khan, S. Auluck, RSC Adv. 4 (2014) 11967–11974.